



Published in final edited form as:

Biomaterials. 2015 October ; 66: 41–52. doi:10.1016/j.biomaterials.2015.07.005.

Dermal delivery of HSP47 siRNA with NOX4-modulating mesoporous silica-based nanoparticles for treating fibrosis

Jingga Morry¹, Worapol Ngamcherdtrakul¹, Shenda Gu¹, Shaun M. Goodyear¹, David J. Castro^{1,2}, Moataz M. Reda¹, Thanapon Sangvanich¹, and Wassana Yantasee^{1,2,*}

¹Department of Biomedical Engineering, Oregon Health and Science University, 3303 SW Bond Ave, Portland, OR 97239, USA.

²PDX Pharmaceuticals, LLC, 24 Independence Ave, Lake Oswego, OR 97035, USA.

Abstract

Fibrotic diseases such as scleroderma have been linked to increased oxidative stress and upregulation of pro-fibrotic genes. Recent work suggests a role of NADPH oxidase 4 (NOX4) and heat shock protein 47 (HSP47) in inducing excessive collagen synthesis, leading to fibrotic diseases. Herein, we elucidate the relationship between NOX4 and HSP47 in fibrogenesis and propose to modulate them altogether as a new strategy to treat fibrosis. We developed a nanoparticle platform consisting of polyethylenimine (PEI) and polyethylene glycol (PEG) coating on a 50-nm mesoporous silica nanoparticle (MSNP) core. The nanoparticles effectively delivered small interfering RNA (siRNA) targeting HSP47 (siHSP47) in an *in vitro* model of fibrosis based on TGF- β stimulated fibroblasts. The MSNP core also imparted an antioxidant property by scavenging reactive oxygen species (ROS) and subsequently reducing NOX4 levels in the *in vitro* fibrogenesis model. The nanoparticle was far superior to n-acetyl cysteine (NAC) at modulating pro-fibrotic markers. *In vivo* evaluation was performed in a bleomycin-induced scleroderma mouse model, which shares many similarities to human scleroderma disease. Intradermal administration of siHSP47-nanoparticles effectively reduced HSP47 protein expression in skin to normal level. In addition, the antioxidant MSNP also played a prominent role in reducing the pro-fibrotic markers, NOX4, alpha smooth muscle actin (α -SMA), and collagen type I (COL I), as well as skin thickness of the mice.

*To whom correspondence should be addressed: Wassana Yantasee, Ph.D., 3303 SW Bond Ave, Portland, OR 97239, USA., Tel: 503-418-9306, Fax: 503-418-9311, yantasee@ohsu.edu.

Publisher's Disclaimer: This is a PDF file of an unedited manuscript that has been accepted for publication. As a service to our customers we are providing this early version of the manuscript. The manuscript will undergo copyediting, typesetting, and review of the resulting proof before it is published in its final citable form. Please note that during the production process errors may be discovered which could affect the content, and all legal disclaimers that apply to the journal pertain.

Contributions

JM, SMG, and SG performed the *in vitro* experiments. JM, DJC, and SMG conducted the *in vivo* experiments. WN, MR, and TS synthesized and characterized the nanoparticles. JM, DJC, WN, and WY analyzed results and wrote the manuscript.

Competing financial interests

OHSU, JM, WN, DJC, and WY have a significant financial interest in PDX Pharmaceuticals, LLC, a company that may have a commercial interest in the results of this research and technology. This potential personal and institutional conflict of interest has been reviewed and managed by OHSU.

Keywords

Dermal delivery; fibrosis; HSP47; NOX4; MSNP; siRNA

1. Introduction

Fibrosis is a complex disease characterized by increased oxidative stress [1, 2], persistent inflammation [3, 4], elevated levels of profibrotic and proinflammatory cytokines [5–7], and an excessive synthesis and accumulation of extracellular matrices, mainly consisting of collagen [6, 7]. Fibrosis can occur in a wide spectrum of organs (e.g., lung, liver, skin, heart), and, if left untreated, can result in organ failure and death [8]. Notably, nearly 45% of all naturally-occurring deaths in the western world are attributed to some form of fibrotic disease [8, 9]. Current approaches to treating fibrosis in patients have mainly focused on antagonizing fibrosis-associated inflammation using drugs such as corticosteroids, which is often ineffective [10] and lead to unwanted side effects with long term use [11, 12]. Several clinical studies have focused on either suppressing oxidative stress (e.g., with N-acetylcysteine (NAC) [13], α -tocopherol (vitamin E) [14]), or reducing pro-fibrotic cytokines/genes (e.g., with monoclonal antibody against TGF- β [15], tyrosine kinase inhibitor, imatinib [16]). However, these attempts have not provided a satisfactory therapeutic index.

We hypothesize that managing both pro-fibrotic genes along with oxidative stress may have greater impact for treating fibrosis than managing just one factor. A nanoparticle platform could be designed to accomplish both. Recently, several inorganic nanoparticles (nickel [17], platinum [18–20], ceria [21, 22], yttria [22], and mesoporous silica [23, 24]) have been shown to possess intrinsic antioxidant properties. Among them, mesoporous silica nanoparticles (MSNPs) are considered the most promising due to their high biocompatibility (low toxicity *in vivo* as well as the ability to be degraded into soluble silicic acid species and cleared by the kidneys) [25–27] and ease of surface modification. Furthermore, MSNPs have been shown to decrease reactive oxygen species (ROS) [23, 24, 28] and attenuate NOX4 mRNA expression in melanoma cells *in vitro* [24]. NOX4 is an enzyme that provides the endogenous source of ROS by catalyzing the reduction of oxygen in cells to hydrogen peroxide [29] (Fig. 1) and has also been implicated in the pathogenesis of various organ fibroses such as liver [30], lung [1, 31, 32], and dermal fibrosis [33, 34]. NOX4 can also be generated downstream of the TGF- β pathway [35], activated in the presence of ROS-producing inflammatory cells (e.g., neutrophils, macrophages) [5] during fibrosis as shown in Fig. 1. Suppression of NOX4 activity with a NOX inhibitor diphenyleneiodonium chloride (DPI) [31, 32], siRNA [31, 32], or the antioxidant N-acetylcysteine (NAC) [31], were shown to decrease the expression of alpha smooth muscle actin (α -SMA) and collagen I (COL I) in fibroblasts collected from pulmonary fibrosis patients [31] and in a bleomycin-induced lung injury mouse model [32]. Thus, we hypothesize that MSNP can remove ROS from the vicinity of the fibrotic tissue and alleviate fibrogenesis by reducing NOX4-associated fibroblast activation and proliferation.

The other benefit of MSNPs is their versatility as a delivery platform for drugs and small interfering RNA (siRNA). Gene silencing using siRNA has long been employed to study the roles of genes in various biological pathways. Although promising, the utility of siRNA as a therapeutic agent has been hindered by its poor cellular uptake and short half-life [36]. Multiple MSNP-based platforms for siRNA delivery have been tested for cancer treatment [37–40]. We have constructed an MSNP-based platform with optimized particle size and chemical modification to overcome barriers of systemic siRNA delivery to solid breast tumors [41]. Specifically, we utilized a co-polymer of PEI-PEG coating on the surface of 50nm-MSNP core to create MSNP-PEI-PEG nanoparticles. The PEI layer electrostatically binds the negatively charged siRNA, and the PEG layer protects siRNA from enzymatic degradation. Anti-HER2 antibody has previously been attached at the end of PEG for targeted delivery to HER2-positive breast cancer [41]. Because siRNA is loaded last through electrostatic interaction (based on the phosphodiester backbone of siRNA, which is sequence-independent) and resides on the outer surface, we can tailor the nanoconstructs for any gene target deemed essential for disease progression, enabling personalized medicine.

In this study, we harness the intrinsic antioxidant property of the MSNPs while assessing the added benefit of a gene silencing strategy to combat fibrogenesis. We chose heat shock protein 47 (HSP47) as the initial siRNA target because it plays an important role in collagen homeostasis (Fig. 1). HSP47 is a collagen-specific molecular chaperone that presides in the endoplasmic reticulum and binds to procollagen molecule to ensure its proper assembly before secretion into the extracellular space [42]. Elevated levels of HSP47 have been particularly observed in fibrotic tissues of patients suffering from systemic sclerosis [43], dermal [44], kidney [45], lung [46], and liver fibrosis [47]. Thus, reducing levels of HSP47 could potentially hinder collagen accumulation and halt the progression of fibrosis. Several preclinical studies have shown that treatment with siRNA against HSP47 could reduce the deposition of collagen into the extracellular matrices in *in vivo* models of liver [48], pancreatic [49], and peritoneal fibrosis [50]. One study showed that siRNA against HSP47, when delivered with vitamin A-coupled liposomes, could yield promising results for treating liver fibrosis in an *in vivo* rat model [48] and is currently undergoing a Phase Ib/II clinical trial (NCT02227459, Nitto Denko Corp., no published clinical trial results yet). This provides evidence that HSP47 may be an excellent gene target for anti-fibrotic treatment.

Intradermal siRNA delivery is an attractive strategy for treating cutaneous pathological conditions due to reduced risk of systemic toxicity. Two phase I clinical trials have been recently completed with encouraging results, one involving intradermal injections of siRNA against keratin 6a [51] to treat pachyonychia congenita (PC) and the other involving injection of siRNA against connective growth tissue factor (CTGF) to reduce dermal scarring in pre-existing hypertrophic scar patients undergoing scar revision surgery (RXI-109, RXi Pharmaceuticals, Westborough, MA). However, local delivery of nanoparticle-based siRNA delivery system has not been attempted for treatment of dermal fibrotic diseases such as scleroderma.

We demonstrate, for the first time, a nanoparticle platform capable of delivering siRNA with intrinsic antioxidant properties for treating fibrosis. For efficacy evaluation, we exploited the well-established TGF- β -induced *in vitro* fibrosis model. We also utilized the dermal fibrosis

mouse model developed by repeated injections of bleomycin to mouse skin [52], which mimicked the pathologic process underlying scleroderma in human.

2. Materials and Methods

2.1. Synthesis of MSNP-PEI-PEG Nanoparticles and siRNA Loading

Mesoporous silica nanoparticles (MSNPs) of 50 nm in size were synthesized and surface-modified as in our previous report [41]. Briefly, 0.15 M cetyltrimethylammonium chloride (CTAC) surfactant was mixed with 350 μ L triethanolamine (TEA) in 125 mL of water at 95 $^{\circ}$ C. Then, 3 mL of tetraethoxysilane (TEOS) was added and the mixture was stirred for one hour. Nanoparticles were recovered from the suspension by centrifugation (60 min, 15 $^{\circ}$ C, 13,000 rpm), washed with ethanol twice and dried overnight in a desiccator. They were then re-suspended and refluxed in acidic methanol (0.6 M HCl in methanol) to remove CTAC. MSNPs were then washed with ethanol and dried in a desiccator. For PEI modification, PEI (branched, 10 kDa) was added into MSNP in absolute ethanol at a weight ratio of 1:4 of PEI per MSNP, and the mixture was shaken at 300 rpm for 3 hr at room temperature. The MSNP-PEI was then centrifuged at 15,000 rpm for 30 min and resuspended in the ethanol solution containing free PEI and 0.2 mg dithiobis(succinimidyl propionate) (DSP, ThermoFisher, Waltham, MA) as a crosslinker. The solution was shaken for another 40 minutes. For PEG modification, 50 mg of mPEG-5kDa-NHS (JenKem, Plano, TX) was conjugated to the primary amines of MSNP-PEI (10 mg) in 1X PBS solution (pH 7.2) under stirred conditions overnight. The MSNP-PEI-PEG was then washed with the PBS solution and kept in this solution until use. The loading of siRNA onto MSNP-PEI-PEG was performed in the same PBS solution at room temperature under 1 hr of shaking. A nanoparticle to siRNA mass ratio of 25 (complete binding level) was used throughout the study. All reagents were from Sigma Aldrich (St. Louis, MO), unless specified otherwise.

2.2. Characterization of Nanoparticles

Mesoporous silica nanoparticle (MSNP) cores were measured for primary (dry) size by a Transmission Electron Microscope (Philips/FEI Tecnai TEM, Hillsboro, OR). After the chemical modification, the material was measured for hydrodynamic size in pH 7.2 PBS with a Zetasizer (Malvern, Westborough, MA). PEI and PEG loadings were quantified by a thermogravimetric analyzer (TGA Q50, TA Instruments, New Castle, DE). siRNA loading was quantified by fluorescent detection of dye-tagged siRNA as well as gel electrophoresis.

2.3. Cell Culture and Primary Dermal Fibroblast Isolation

Primary murine dermal fibroblasts were harvested from skin biopsies (6-mm diameter biopsy punch) obtained from 4 normal and 4 bleomycin-treated C3H/HeJ mice (as described in *section 2.9*). Following procedure described by Takashima et al. [53], excised skin was held on ice in Hank's buffered saline solution with 1% pen-strep, while the fat tissues were removed prior to mincing the remaining skin into small pieces. 2 mL of 100 U/mL collagenase type I (Worthington Biochemical Corp., Freehold, NJ) was added into the minced tissues, and the suspension was stirred at 37 $^{\circ}$ C for 1 hr. Dissociated fibroblast cells, designated "normal fibroblast" from normal skin and "bleo fibroblast" from bleomycin-treated skin, were pelleted at 1000 rpm for 5 min. The cell pellet was then re-suspended in

warm DMEM (Cellgro, Manassas, VA) supplemented with 10% FBS and 1% pen-strep. The cell suspension was then filtered through a 40 μm cell strainer (BD Falcon, BD Biosciences, San Jose, CA) before plating in the same medium. The cell cultures were maintained for 3 to 9 passages, but passages 7 and 8 were mostly utilized. The normal and bleo-fibroblast cultures were characterized for mRNA levels of HSP47, COL I, and α -SMA and stained for vimentin (fibroblast-specific marker [54]) and α -SMA (myofibroblast marker [55]) by immunohistochemistry (Supplementary Fig. S1).

Murine embryonic fibroblast cell line, NIH/3T3, was cultured in DMEM supplemented with 10% FBS and 1% pen-strep. Adult human dermal fibroblast cell line (HDFa, Life Technologies, Carlsbad, CA) was cultured in Medium 106 (Life Technologies) supplemented with Low Serum Growth Supplement (LSGS, Life Technologies) per the manufacturer's recommendation. All cell lines were maintained at 37 $^{\circ}\text{C}$ and 5% CO_2 humidified incubator. Two to four *in vitro* experimental replicates were performed for each experiment with at least three analytical replicates per each sample.

2.4. Cellular Uptake of Nanoparticles

For cellular uptake experiments, primary murine dermal fibroblast cells (normal skin) were seeded at 8,000 cells/well on 96-well plates overnight in complete DMEM medium (DMEM + 10% FBS). The cells were then serum-starved in DMEM with 0.5% FBS on the next day prior to treatment with either 50 nM of non-targeting siRNA (siSCR, see Supplementary Table S1 for siRNA sequence) conjugated with DyLight677 delivered by MSNP-PEI-PEG (17.5 $\mu\text{g}/\text{mL}$) or DharmaFECT (0.5 $\mu\text{L}/\text{well}$ in 100 μL medium, DharmaFECT-1, Thermo Scientific, Lafayette, CO). After 24 hr of incubation, the cells were washed three times with PBS to remove non-internalized nanoparticles and stained with cell-permeant Hoechst (33342, Life Technologies) dye at 37 $^{\circ}\text{C}$ for 30 min before fixation in 4% paraformaldehyde (PFA) for 15 min. Internalized DyLight677-siRNA was detected using a fluorescence microscope (EVOS FL, Life Technologies). Fluorescence intensity of DyLight677 was normalized over the total cell number (Hoechst-positive) and analyzed using Cell Profiler open-source image analysis software (Broad Institute, Cambridge, MA).

2.5. Intracellular ROS Assay

To measure cellular ROS induction by nanoparticles, primary murine dermal fibroblast cells were pre-treated with either siSCR-MSNP-PEI-PEG, siSCR-DharmaFECT, (prepared in a similar manner as 2.4), or 2 mM of N-acetylcysteine (NAC, Sigma Aldrich) antioxidant. After 24 hr, 100 μM of menadione was added into each well for 1 hr to induce oxidative stress. At the end of the incubation period, the cellular ROS was assayed using CellROX[®] green reagent (Life Technologies) following the manufacturer's protocol. The fluorescence intensity of CellROX[®] green was normalized over the total cell number (Hoechst-positive) and analyzed using Cell Profiler open-source image analysis software.

2.6. DPPH Free Radical Scavenging Assay

The 2, 2-diphenyl-1-picrylhydrazyl (DPPH, Sigma Aldrich) free radical scavenging assay was used to determine the antioxidant property of the nanoparticles. This assay is based on the reduction of the odd electron on the nitrogen atom in DPPH by antioxidants [56].

Briefly, various concentrations (from 0–500 $\mu\text{g}/\text{mL}$) of MSNP core, PEI, MSNP-PEI-PEG, and NAC were prepared in PBS solution and administered in triplicate in a 96-well plate (cell-free) followed by the addition of an equal volume of 0.5 mM DPPH (in ethanol). The mixture was then incubated in the dark at room temperature under shaking (300 rpm) for 15 min. Absorbance (abs.) was read at 517 nm using a TECAN spectrophotometer (TECAN US Inc., Research Triangle Park, NC). The percentage of DPPH scavenging radical was calculated as follows:

$$\%DPPH \text{ scavenging} = \left(\text{abs. of blank} - \frac{\text{abs. of sample}}{\text{abs. of blank}} \right) \times 100$$

2.7. In vitro Evaluation of siHSP47 and siNOX4

siRNA against HSP47 (siHSP47) and NOX4 (siNOX4) were screened from 3–4 sequences as summarized in Supplementary Table S1. Once the best siRNA sequence was identified (Supplementary Fig. S2), it was used for *in vitro* gene silencing under TGF- β stimulation conditions as follows. Primary murine dermal fibroblast cells were seeded on a 96-well plate (8,000 cells/well) or on a 6-well plate (150,000 cells/well) overnight in complete medium. On the next day, the medium was replaced with DMEM with 0.5% FBS for 16 hr. Cells were then transfected with 50 nM siRNA on 17.5 $\mu\text{g}/\text{mL}$ of MSNP-PEI-PEG or DharmaFECT (0.5 $\mu\text{L}/\text{well}$). After 24 hr, cells were washed once and the culture medium was replaced with fresh medium (DMEM with 0.5% FBS) containing 10 ng/mL TGF- β (Peprotech Inc., Rocky Hill, NJ) and incubated either for another 24 hr (mRNA detection) or 72 hr (protein detection). For bleo-fibroblast cells, the MSNP-PEI-PEG and DharmaFECT treatments were done in a similar manner as above, but without TGF- β stimulation. The HSP47, NOX4, COL I, and α -SMA protein expressions of the treated cells were quantified with either immunofluorescence imaging (IF) or Western Blot, while their mRNA levels were quantified with qRT-PCR. These three methods are summarized in Supplementary Methods.

2.8. Cell Viability Assay

The viability of the cells treated as described in 2.7 was also determined at 96 hr post transfection using CellTiter-Glo[®] Luminescent Cell Viability Assay (Promega, Madison, WI) following the manufacturer's protocol. The data were reported as the fold change over the untreated control.

2.9. SiHSP47-MSNP-PEI-PEG Nanoparticle Treatment of Bleomycin-Induced Scleroderma Mouse Model

The induction of dermal fibrosis (scleroderma) with bleomycin in mice followed the procedure described by Yamamoto et al. [52]. The experimental protocol was approved by the Institutional Animal Care and Use Committee (IACUC) of Oregon Health and Science University (OHSU). Specifically, 6–7 week old C3H/HeJ mice (Jackson Laboratories, Bar Harbor, ME) were intradermally injected with 100 μL of 0.5 mg/mL bleomycin in PBS (APP Pharmaceuticals, Melrose Park, IL) at the same location on the shaved back of mice every other day for 4 weeks (3 times weekly). Concurrently, mice (6–7 per group) were

injected with 50 μ L of PBS suspension containing siSCR- or siHSP47-MSN-PEI-PEG at the dose of 220 μ g nanoparticles and 0.65 nmol as siRNA. The siRNA dose was adapted from the reported intradermally injected siRNA doses to mice [57, 58]. Treatments were done twice a week on alternate days with bleomycin injection for a total of 8 treatments over 4 weeks. A positive control group received bleomycin and saline injections. All mice were sacrificed 4 days after the last injection with the siRNA-nanoparticle treatment.

2.10. Histological Analysis of Bleomycin-Induced Scleroderma Mouse Skin

Skin tissues from the region of injection, about 6 mm in diameter, were collected by biopsy punch and fixed in 4% PFA prior to processing and paraffin embedding. 5 μ m-thick paraffin-embedded sections were used for H&E stain to determine dermal thickness. Six images were taken per tissue section with the EVOS-XL (Life Technologies) microscope at x200 magnification. Dermal thickness was measured as the distance between the epidermal-dermal junction and the dermal-adipose layer junction, and the data were presented as the fold change over the untreated control.

2.11. Immunohistochemistry for Pro-fibrotic Markers on Skin Sections

Deparaffinized and rehydrated skin sections were subjected to heat-mediated antigen retrieval in citrate buffer (10 mM, pH 6.0) for 30 min. The tissue sections were blocked with 5% goat-serum (Vector Laboratories Inc., Burlingame, CA) for 1 hr at room temperature. Slides were then incubated with primary antibodies at 4 °C overnight, secondary antibodies for 1 hr at room temperature, and mounted with Prolong Gold Antifade reagent with DAPI (P-3691, Invitrogen, Carlsbad, CA). A summary of antibodies used and working dilution is provided in Supplementary Methods. Six images were taken per tissue section per animal with the EVOS FL fluorescence microscope at x200 magnification. The total fluorescence intensity of the tissue sections was normalized over the total image area and analyzed using Cell Profiler open-source image analysis software. For the measurement of COL I and α -SMA positive area, the 'MeasureImageAreaOccupied' module in Cell Profiler software was used and calculated as the relative area occupied by the protein of interest (COL I or α -SMA) to the total area of the tissue.

2.12. Statistical Analysis

Experiments were performed in triplicate with results presented as mean \pm standard deviation. Data were analyzed using one-way ANOVA with post-hoc Dunnett's multiple comparison test with significance set at $p < 0.05$. Graphpad Prism 6.0 software (GraphPad software Inc., San Diego, CA) was utilized for statistical analyses.

3. Results and Discussion

3.1. Synthesis and Characterization of Nanoparticles (MSN-PEI-PEG)

Transmission electron micrograph (TEM, Fig. 2A) showed that the MSNP core had porous morphology with particle size of 47 ± 4 nm in diameter. Layer-by-layer coating with polyethyleneimine (PEI) and polyethylene glycol (PEG) (see schematic representation in Fig. 2B) was confirmed by Thermogravimetric Analysis (TGA). TGA analysis established the amount of attached PEI and PEG on MSNP to be 13.5% and 18.2% by dry weight of the

whole nanoparticle, respectively. After the surface modification, MSNP-PEI-PEG has a hydrodynamic size of 104 ± 1.7 nm (Fig. 2C) and zeta potential of 15.1 ± 0.7 mV (in 10 mM NaCl). The nanoparticle had a small polydispersity index (PDI) of 0.19, showing narrow size distribution. Even after siRNA loading, the particle size remains unchanged (Fig. 2C). As shown in Fig. 2B, the siRNA is bound to PEI and is protected underneath the PEG layer. As a result, the siRNA was 100% protected against serum enzymes for at least 24 hr (measured in 50% human serum) [41].

3.2. Cellular Uptake of siRNA-Nanoparticles (MSNP-PEI-PEG)

Supplementary Fig. S3A shows a non-uniform cellular uptake of siSCR (siSCR is a non-targeting siRNA) in primary murine dermal fibroblasts 24 hr post-transfection with DharmaFECT. In contrast, transfection with the MSNP-PEI-PEG nanoparticles was very uniform. The siSCR was tagged with DyLight677 to allow for fluorescent monitoring. The cellular signal of dye-tagged siRNA increased by $76 \pm 31\%$ with nanoparticle delivery versus $49 \pm 56\%$ by DharmaFECT delivery (vs. the untreated control, Fig. S3B). The non-uniform cellular uptake is likely attributed to the large particle size of siRNA-DharmaFECT (446 nm in nominal size with the range of 190–955 nm vs. the 100 nm size of siRNA-nanoparticles with the range of 44–255 nm) (Fig. S3C).

3.3. ROS Scavenging Ability of Nanoparticles (MSNP-PEI-PEG)

The antioxidant properties of bare MSNP (without chemical modification) in a human melanoma [23, 24] and mouse embryonic fibroblast [28] cell line have been reported as described previously. To assess the antioxidant property of MSNP-PEI-PEG in our cells of interest (murine dermal fibroblasts), we measured the ROS level after exposing the cells to MSNP-PEI-PEG overnight followed by 1-hr menadione-induced oxidative stress. Menadione (2-methyl-1,4-naphthoquinone) is a chemical compound known to generate intracellular ROS [59]. Such intracellular ROS could be measured by CellROX Green reagent as shown in Figs. 3A and B. The cellular ROS was increased 7.6-fold after 1 hr of menadione exposure. However, pretreatment of the cells with MSNP-PEI-PEG decreased ROS production to the non-menadione level, while DharmaFECT had little effect. The MSNP-PEI-PEG effect was similar to that obtained by an established antioxidant, N-acetylcysteine (NAC). Note that siSCR was used on the nanoparticles to maintain a similar surface charge of the intended final nanoconstruct without imparting a gene silencing effect.

Reduction of ROS by our nanoparticles was thought to be due to the MSNP core and not the cationic PEI coating. We confirmed the free radical scavenging ability of the materials utilizing the cell free DPPH assay. Fig. 3C shows that bare MSNP displayed higher scavenging ability than MSNP-PEI-PEG, while PEI alone displayed very little effect. NAC was used as the positive control. In addition, we also observed lower ROS activity when NIH/3T3 mouse embryonic fibroblast cells were exposed to the MSNP-PEI-PEG nanoparticles in the presence of H_2O_2 for up to 6 hr (Supplementary Fig. S4). Although MSNP-PEI-PEG had lower scavenging ability than bare MSNP, the PEI-PEG layer is needed. PEI is needed for binding to siRNA, promoting cell entrance (via adsorptive endocytosis), and endosomal escape of siRNA via proton sponge effects [60], while PEG layer is needed for protecting siRNA from blood enzyme degradation [41].

3.4. Effect of MSNP-PEI-PEG on TGF- β -stimulated Dermal Fibroblast Cells and Scleroderma-like Fibroblasts

In scleroderma patients, elevation of TGF- β [61], NOX4 expression [34], and ROS [62] have been observed in dermal fibrotic lesions. In the previous section, MSNP-PEI-PEG nanoparticles were able to reduce cellular ROS. Next, we assess their ability to reduce NOX4 levels using an *in vitro* TGF- β -induced model. TGF- β is one of the major profibrotic growth factors and could stimulate fibroblast proliferation as well as its transdifferentiation to myofibroblast [7, 63, 64]. After TGF- β stimulation of primary murine dermal fibroblasts, we observed a pronounced up-regulation in the protein expression of NOX4 (2.2-fold), HSP47 (1.5-fold), COL I (2.5-fold), and α -SMA (5.6-fold) (vs. untreated control) in Figs. 4A and B. Cell proliferation also increased by 1.9-fold. However, pre-treatment with siSCR-MSNP-PEI-PEG significantly decreased the expression of NOX4, HSP47, COL I, and α -SMA, while siSCR-DharmaFECT had little effect. In particular, NOX4 and HSP47 protein expression returned to the level prior to TGF- β stimulation. These effects were also confirmed at the mRNA level (Supplementary Fig. S5). Similar to section 3.3, siSCR was used to maintain a similar surface charge of the intended final nanoconstruct without imparting a gene silencing effect as shown with DharmaFECT (Fig. 4).

The ability of the MSNP-PEI-PEG nanoparticle to reduce NOX4 and other pro-fibrotic markers was further validated in scleroderma-like fibroblast cells. The cells were harvested from the skin of a mouse receiving intradermal bleomycin injections for 4 weeks, subsequently termed as “bleo-fibroblast”. Thus, these cells were already activated and did not require pre-treatment with TGF- β to trigger a fibrotic response prior to nanoparticle treatment. The bleo-fibroblast cells showed positive staining for the myofibroblast marker α -SMA (Supplementary Fig. S1A) and pronounced up-regulation of mRNA levels for HSP47, NOX4, COL I, and α -SMA (Fig. 4C and Supplementary Fig. S1C) in a similar manner as the TGF- β stimulated cells in Figs. 4A–B and 5. Bleomycin injection in mouse skin has been shown to induce macrophage accumulation and local TGF- β production [65, 66]. MSNP-PEI-PEG (with siSCR) treatment on these cells resulted in significant reduction in NOX4, COL I, and α -SMA mRNA expression ($p < 0.0001$) compared to the untreated counterpart (Fig. 4C). NAC treatment at 2 mM could reduce NOX4 mRNA expression to the same extent as MSNP-PEI-PEG, but was unable to reduce the levels of COL I and α -SMA. A much higher dose of NAC (20 mM) was reported to be able to inhibit these pro-fibrotic markers [34, 62]. However, such a high dose of NAC is impossible to achieve *in vivo* without toxicity concerns. An estimated 5010 mg/kg loading dose (e.g., first 60 min) and 2250 mg/kg maintenance dose (e.g., next 4 hr) are needed to reach 10 mM concentration in blood based on the pharmacokinetic data of NAC in human volunteers [67], but NAC is prescribed at only 150 mg/kg loading dose and 50 mg/kg maintenance dose (i.v.) (NAC, Acetadote®, package insert) or 600-mg oral dose (three times daily) for pulmonary fibrosis patients in the PANTHER-IPF trial [13]. This may be one of the reasons why oral monotherapy of NAC in pulmonary fibrosis patients did not show any beneficial effects and was also accompanied by a higher rate of cardiac events compared to the placebo treatment [13]. In short, a much lower dose (17.5 mg/L) of MSNP-PEI-PEG was found to yield greater anti-fibrotic effects than NAC (~300 mg/L).

3.5. Role of NOX4 and HSP47 in Fibrogenesis

The involvements of both HSP47 and NOX4 in fibrogenesis are complex and have been summarized in Fig. 1. Following tissue injury, the activated leukocytes (macrophages and neutrophils) induce ROS generation and secrete pro-fibrotic cytokines such as TGF- β [5]. The released TGF- β then triggers the synthesis and up-regulation of HSP47 [68] and NOX4 [35, 69, 70] in fibroblast cells. Overexpression of NOX4 induces intracellular ROS [29, 70], while the overexpression of HSP47 induces collagen synthesis (through excessive processing of pro-collagen molecules) [42]. Furthermore, NOX4 has been shown to induce the differentiation of fibroblasts to myofibroblasts [32, 71] and modulates collagen synthesis *in vitro* under TGF- β stimulation [69]. Myofibroblasts, in turn, secrete TGF- β in an autocrine fashion to further induce the activation and proliferation of the fibroblast cells [71].

MSNP-PEI-PEG treatment decreased not only NOX4 but also HSP47 protein expression (Fig. 4). However, the relationship between NOX4 and HSP47 has not been clearly elucidated. In order to understand the relationship between these two genes, we exploited siNOX4 or siHSP47 in separate studies without the use of nanoparticles. After the best sequence for siNOX4 and siHSP47 were identified (see Supplementary Fig. S2), they were transfected using DharmaFECT in primary dermal fibroblast cells for 24 hr prior to TGF- β stimulation. As shown in Fig. 5A, knocking down NOX4 with siNOX4 also resulted in down-regulation of HSP47. This is not the result of an off-targeting effect of the siNOX4 sequence as both the antisense and sense strands do not show sequence homology to murine HSP47 mRNA sequence. In addition to NOX4 knockdown, COL I and α -SMA were also down-regulated. The data suggest that NOX4 may act as an upstream effector of HSP47. Oxidative stress could induce HSP47 production in several *in vitro* systems [72, 73], thus it is possible that silencing NOX4 reduces oxidative stress, which, in turn, lowers the expression of HSP47.

This relationship was further validated upon knocking down HSP47 (with siHSP47) which still significantly reduced COL I and α -SMA levels without altering NOX4 levels (Fig. 5B). Hence, we hypothesize that, in addition to down-regulating NOX4 with our antioxidant nanoparticles, silencing HSP47 gene (with siHSP47) may have enhanced anti-fibrotic efficacy beyond managing the individual genes alone.

3.6. In vitro HSP47 Gene Knock-down Efficacy by siHSP47-MSNP-PEI-PEG

We investigated the ability of MSNP-PEI-PEG nanoparticles in delivering siHSP47 in TGF- β -stimulated dermal fibroblasts and benchmarked it against the traditional DharmaFECT-mediated transfection. Delivery of siHSP47 with our MSNP-PEI-PEG potently silenced HSP47 gene expression by 95% at 48 hr post-transfection, whereas transfection with DharmaFECT could only reduce HSP47 gene expression by 81% (Supplementary Fig. S5). This correlated to an 86% reduction in HSP47 protein expression at 96 hr post transfection with the siHSP47-MSNP-PEI-PEG compared to 63% achieved with siHSP47-DharmaFECT (Figs. 6A–B). Furthermore, the siSCR-MSNP-PEI-PEG could also decrease the HSP47 mRNA and protein expressions by 72% and 21%, respectively, demonstrating the ability of the MSNP-PEI-PEG nanoparticles in reducing HSP47.

To test if our nanoparticles have the ability to reduce HSP47 expression in activated fibroblast cells (without TGF- β stimulation), a similar experiment was performed with the derived bleo-fibroblast cells. As shown in Supplementary Fig. S6, treatment with siHSP47-MSNP-PEI-PEG resulted in more than 90% HSP47 mRNA knockdown at 48 hr. In comparison, NAC at high dose (20 mM) could only reduce HSP47 level by 48%. In agreement with the findings in TGF- β -stimulated cells, MSNP-PEI-PEG could also decrease 20% of HSP47 mRNA expression in the bleo-fibroblast cells.

There was also no significant cytotoxicity associated with our nanoparticle treatment as shown in Fig. 6C. Furthermore, the nanoparticles had no significant efficacious dose for 24 and 48 hr (Supplementary Fig. S7). Therefore, the nanoparticle should serve as a safe and effective siRNA delivery system to the cells.

In summary, our *in vitro* findings so far have indicated that MSNP-PEI-PEG nanoparticle could serve as a superior siRNA carrier and can be therapeutic with regard to fibrosis treatment. The benefit of knocking down HSP47 with siHSP47 was also evident. These results prompted us to validate our *in vitro* finding with an *in vivo* mouse model.

3.7. In Vivo Evaluation of siHSP47-MSNP-PEI-PEG: Skin Thickness

In order to further examine the therapeutic potential of our siHSP47-nanoparticles *in vivo*, we employed a well-accepted bleomycin-induced dermal fibrosis (scleroderma) mouse model [52]. Given intradermally, bleomycin induces toxicity (since skin lacks bleomycin hydrolase enzyme to metabolize bleomycin) and leads to the induction of ROS and pro-inflammatory cytokines (including TGF- β) to the skin [74].

We intradermally injected the siHSP47- or siSCR-MSNP-PEI-PEG nanoparticles to the shaved back of the mice on a twice-weekly schedule and on alternate days of bleomycin administration over the course of 4 weeks as shown in Fig. 7A. We also confirmed in a separate experiment that there was no binding of bleomycin onto the nanoparticles, which may have blocked the fibrogenesis effect of bleomycin (data not shown).

After the study was completed, H&E stains of skin sections were analyzed as shown in Figs. 7B and 7C. The bleomycin treatment increased the dermal thickness by 42% ($p < 0.001$ vs. untreated). Treatment of siHSP47-MSNP-PEI-PEG nanoparticles to the bleomycin-treated mice resulted in the reduction of dermal thickness by 19% ($p < 0.01$ vs. bleomycin alone), which brought the value down to the untreated level ($p=0.38$). Treatment of siSCR-MSNP-PEI-PEG nanoparticle could also decrease the dermal thickness by 7%, but not significantly different from bleomycin alone ($p=0.21$) and could not bring the value down to the untreated level ($p < 0.03$). These data indicated beneficial treatment of siHSP47-MSNP-PEI-PEG nanoparticle over MSNP-PEI-PEG alone.

3.8. In Vivo Evaluation of siHSP47-MSNP-PEI-PEG: Protein Characterization

To examine whether siHSP47-MSNP-PEI-PEG can successfully silence HSP47 expression in the skin, we analyzed skin specimens harvested from mice treated as described in section 3.7. Immunofluorescence detection was used for protein characterization as shown in Fig. 8A, and quantified in Figs. 8B–E. There was a clear up-regulation of HSP47 by 170% in the

skin of mice treated with bleomycin (Fig. 8B). The siHSP47-MSN-PEI-PEG treatment was able to reduce bleomycin-induced HSP47 expression to levels similar to the untreated control ($p=0.28$). The siSCR-MSN-PEI-PEG treatment also decreased the HSP47 expression but to a much lesser extent and with less precision (larger standard deviation) than the siHSP47-MSN-PEI-PEG counterpart. It could not bring the HSP47 level down to the untreated level ($p < 0.0001$). As anticipated from the *in vitro* studies, the MSN-PEI-PEG could reduce bleomycin-induced NOX4 expression effectively to the untreated level regardless of siSCR or siHSP47 ($p < 0.0001$) (Fig. 8C).

Bleomycin injection to the skin increased the α -SMA- and COL I-positive area by 2.7- and 1.6-fold compared to the untreated level, respectively. With siHSP47-MSN-PEI-PEG treatment, the area positive for α -SMA was reduced by 49% ($p < 0.01$) as compared to the bleomycin group (Fig. 8D). Likewise, COL I-positive area for the siHSP47-nanoparticle treatment was reduced by 51% (Fig. 8E), which restores it to the normal levels ($p=0.99$). The siSCR-MSN-PEI-PEG effects on the reduction of the profibrotic markers (vs. bleomycin alone) were less substantial; 24% ($p=0.57$) for α -SMA and 19% ($p=0.25$) for COL I, respectively. In addition, the mRNA analysis from the skin tissues collected from the siHSP47-MSN-PEI-PEG treated mice confirmed our findings in Fig. 8. As shown in Supplementary Fig. S8, siHSP47-MSN-PEI-PEG treatment showed significant reduction in HSP47 ($p < 0.05$), COL I ($p < 0.0001$), and α -SMA ($p < 0.05$) levels vs. bleomycin treatment alone. In agreement with the *in vitro* study, the siSCR-MSN-PEI-PEG treatment also showed significant COL I and α -SMA reduction. However, the reduction of COL I was greater with siHSP47-MSN-PEI-PEG treatment (94% vs. 70%). In conclusion, there is a clear advantage of siHSP47-MSN-PEI-PEG nanoparticle over MSN-PEI-PEG nanoparticle alone. Lastly, the cellular internalization of the nanoparticle in the dermis region of the mouse skin was observed by TEM as shown in the Supplementary Fig. S9.

Conclusions

In this work, we described the roles of ROS, NOX4, and HSP47 in fibrogenesis and developed a nanoparticle platform to modulate all three effectors in order to treat fibrosis. We show that our MSN-PEI-PEG nanoparticles could efficiently deliver siRNA to knock-down HSP47 expression *in vitro* and *in vivo*. In addition, the nanoparticle carrier itself could reduce ROS and NOX4 production, owing to the antioxidant property of the MSN core, which is by far superior to NAC. We also elucidate, for the first time, that NOX4 may be an upstream effector of HSP47, which provides the explanation on how our nanoparticle carrier alone could also down-regulate the expressions of HSP47 and the associated fibrotic markers, COL I and α -SMA. The therapeutic impact of MSN-PEI-PEG can be further enhanced by the addition of siRNA against HSP47 as demonstrated in a scleroderma mouse model. Intradermal MSN-PEI-PEG treatment could alleviate skin fibrosis by reducing ROS production, and the antifibrotic effect could be further enhanced by knocking down HSP47 expression with siHSP47. In addition to intradermal delivery reported herein, we have also shown in our most recent work [41] that the nanoparticles could be given intravenously, achieve excellent gene knock-down in solid tumors, and have excellent safety profile. Given the most optimal gene target, our nanoparticles will be able to provide combinatorial treatment for fibrotic diseases of other organs as well as inflammatory diseases.

Supplementary Material

Refer to Web version on PubMed Central for supplementary material.

Acknowledgements

This work was supported by National Institute of General Medical Sciences of the National Institutes of Health (NIH) under award number R01GM089918, National Cancer Institute of NIH under a contract HHSN261201300078C, the Prospect Creek Foundation, and OHSU's Office of The Vice President for Research (VPR). The content is solely the responsibility of the authors and does not necessarily represent the official views of the National Institutes of Health. We would like to thank Drs. Pamela B. Cassidy and Molly Kulesz-Martin for independent reviewing of the manuscript.

References

1. Cheresh P, Kim SJ, Tulasiram S, Kamp DW. Oxidative stress and pulmonary fibrosis. *Biochimica et biophysica acta*. 2013; 1832:1028–1040. [PubMed: 23219955]
2. Gabrielli A, Svegliati S, Moroncini G, Amico D. New insights into the role of oxidative stress in scleroderma fibrosis. *The open rheumatology journal*. 2012; 6:87–95. [PubMed: 22802906]
3. Stramer BM, Mori R, Martin P. The inflammation-fibrosis link? A Jekyll and Hyde role for blood cells during wound repair. *The Journal of investigative dermatology*. 2007; 127:1009–1017. [PubMed: 17435786]
4. Bringardner BD, Baran CP, Eubank TD, Marsh CB. The role of inflammation in the pathogenesis of idiopathic pulmonary fibrosis. *Antioxidants & redox signaling*. 2008; 10:287–301. [PubMed: 17961066]
5. Wynn TA. Integrating mechanisms of pulmonary fibrosis. *The Journal of experimental medicine*. 2011; 208:1339–1350. [PubMed: 21727191]
6. Borg BB, Seetharam A, Subramanian V, Basha HI, Lisker Melman M, Korenblat K, et al. Immune response to extracellular matrix collagen in chronic hepatitis C-induced liver fibrosis. *Liver Transplantation*. 2011; 17:814–823. [PubMed: 21425431]
7. Leask A, Abraham DJ. TGF-beta signaling and the fibrotic response. *FASEB journal : official publication of the Federation of American Societies for Experimental Biology*. 2004; 18:816–827. [PubMed: 15117886]
8. Bitterman PB, Henke CA. Fibroproliferative disorders. *Chest*. 1991; 99
9. Wick G, Grundtman C, Mayerl C, Wimpfissinger TF, Feichtinger J, Zelger B, et al. The immunology of fibrosis. *Annual review of immunology*. 2013; 31:107–135.
10. Rafii R, Juarez MM, Albertson TE, Chan AL. A review of current and novel therapies for idiopathic pulmonary fibrosis. *Journal of thoracic disease*. 2013; 5:48–73. [PubMed: 23372951]
11. Buchman AL. Side effects of corticosteroid therapy. *Journal of clinical gastroenterology*. 2001; 33:289–294. [PubMed: 11588541]
12. Flaherty KR, Toews GB, Lynch JP 3rd, Kazerooni EA, Gross BH, Strawderman RL, et al. Steroids in idiopathic pulmonary fibrosis: a prospective assessment of adverse reactions, response to therapy, and survival. *The American journal of medicine*. 2001; 110:278–282. [PubMed: 11239846]
13. Martinez FJ, de Andrade JA, Anstrom KJ, King TE Jr, Raghu G. Randomized trial of acetylcysteine in idiopathic pulmonary fibrosis. *The New England journal of medicine*. 2014; 370:2093–2101. [PubMed: 24836309]
14. de la Maza MP, Petermann M, Bunout D, Hirsch S. Effects of long-term vitamin E supplementation in alcoholic cirrhotics. *Journal of the American College of Nutrition*. 1995; 14:192–196. [PubMed: 7790695]
15. Denton CP, Merkel PA, Furst DE, Khanna D, Emery P, Hsu VM, et al. Recombinant human anti-transforming growth factor beta1 antibody therapy in systemic sclerosis: a multicenter, randomized, placebo-controlled phase I/II trial of CAT-192. *Arthritis and rheumatism*. 2007; 56:323–333. [PubMed: 17195236]

16. Prey S, Ezzedine K, Doussau A, Grandoulier AS, Barcat D, Chatelus E, et al. Imatinib mesylate in scleroderma-associated diffuse skin fibrosis: a phase II multicentre randomized double-blinded controlled trial. *The British journal of dermatology*. 2012; 167:1138–1144. [PubMed: 23039171]
17. Saikia JP, Paul S, Konwar BK, Samdarshi SK. Nickel oxide nanoparticles: a novel antioxidant. *Colloids and surfaces B, Biointerfaces*. 2010; 78:146–148. [PubMed: 20219331]
18. Nomura M, Yoshimura Y, Kikuri T, Hasegawa T, Taniguchi Y, Deyama Y, et al. Platinum nanoparticles suppress osteoclastogenesis through scavenging of reactive oxygen species produced in RAW264.7 cells. *Journal of pharmacological sciences*. 2011; 117:243–252. [PubMed: 22083043]
19. Onizawa S, Aoshiba K, Kajita M, Miyamoto Y, Nagai A. Platinum nanoparticle antioxidants inhibit pulmonary inflammation in mice exposed to cigarette smoke. *Pulmonary pharmacology & therapeutics*. 2009; 22:340–349. [PubMed: 19166956]
20. Watanabe A, Kajita M, Kim J, Kanayama A, Takahashi K, Mashino T, et al. In vitro free radical scavenging activity of platinum nanoparticles. *Nanotechnology*. 2009; 20:455105–455114. [PubMed: 19834242]
21. Heckert EG, Karakoti AS, Seal S, Self WT. The role of cerium redox state in the SOD mimetic activity of nanocerium. *Biomaterials*. 2008; 29:2705–2709. [PubMed: 18395249]
22. Schubert D, Dargusch R, Raitano J, Chan SW. Cerium and yttrium oxide nanoparticles are neuroprotective. *Biochemical and biophysical research communications*. 2006; 342:86–91. [PubMed: 16480682]
23. Hao N, Yang H, Li L, Li L, Tang F. The shape effect of mesoporous silica nanoparticles on intracellular reactive oxygen species in A375 cells. *New Journal of Chemistry*. 2014; 38:4258–4266.
24. Huang X, Zhuang J, Teng X, Li L, Chen D, Yan X, et al. The promotion of human malignant melanoma growth by mesoporous silica nanoparticles through decreased reactive oxygen species. *Biomaterials*. 2010; 31:6142–6153. [PubMed: 20510446]
25. Shahbazi MA, Herranz B, Santos HA. Nanostructured porous Si-based nanoparticles for targeted drug delivery. *Biomater*. 2012; 2:296–312. [PubMed: 23507894]
26. Godin B, Gu J, Serda RE, Ferrati S, Liu X, Chiappini C, et al. Multistage Mesoporous Silicon-based Nanocarriers: Biocompatibility with Immune Cells and Controlled Degradation in Physiological Fluids. *Controlled release newsletter / Controlled Release Society*. 2008; 25:9–11. [PubMed: 21853161]
27. Asefa T, Tao Z. Biocompatibility of Mesoporous Silica Nanoparticles. *Chemical Research in Toxicology*. 2012; 25:2265–2284. [PubMed: 22823891]
28. Bajenaru L, Berger D, Miclea L, Matei C, Nastase S, Andronescu C, et al. Correlation of the intracellular reactive oxygen species levels with textural properties of functionalized mesostructured silica. *Journal of biomedical materials research Part A*. 2014; 102:4435–4442. [PubMed: 24677796]
29. Nisimoto Y, Diebold BA, Cosentino-Gomes D, Lambeth JD. Nox4: A Hydrogen Peroxide-Generating Oxygen Sensor. *Biochemistry*. 2014; 53:5111–5120. [PubMed: 25062272]
30. Jiang JX, Chen X, Serizawa N, Szyndralewicz C, Page P, Schroder K, et al. Liver fibrosis and hepatocyte apoptosis are attenuated by GKT137831, a novel NOX4/NOX1 inhibitor in vivo. *Free radical biology & medicine*. 2012; 53:289–296. [PubMed: 22618020]
31. Amara N, Goven D, Prost F, Muloway R, Crestani B, Boczkowski J. NOX4/NADPH oxidase expression is increased in pulmonary fibroblasts from patients with idiopathic pulmonary fibrosis and mediates TGFbeta1-induced fibroblast differentiation into myofibroblasts. *Thorax*. 2010; 65:733–738. [PubMed: 20685750]
32. Hecker L, Vittal R, Jones T, Jagirdar R, Luckhardt TR, Horowitz JC, et al. NADPH oxidase-4 mediates myofibroblast activation and fibrogenic responses to lung injury. *Nature medicine*. 2009; 15:1077–1081.
33. Piera-Velazquez S, Jimenez SA. Role of cellular senescence and NOX4-mediated oxidative stress in systemic sclerosis pathogenesis. *Current rheumatology reports*. 2015; 17:473–483. [PubMed: 25475596]

34. Spadoni T, Svegliati Baroni S, Amico D, Albani L, Moroncini G, Avvedimento EV, et al. A reactive oxygen species-mediated loop maintains the increased expression of NOX2 and NOX4 in skin fibroblasts from patients with systemic sclerosis. *Arthritis & rheumatology* (Hoboken, NJ). 2015; 67:1611–1622.
35. Michaeloudes C, Sukkar MB, Khorasani NM, Bhavsar PK, Chung KF. TGF- β regulates Nox4, MnSOD and catalase expression, and IL-6 release in airway smooth muscle cells. *American Journal of Physiology-Lung Cellular and Molecular Physiology*. 2011; 300:L295–L304. [PubMed: 21131394]
36. Dykxhoorn DM, Palliser D, Lieberman J. The silent treatment: siRNAs as small molecule drugs. *Gene therapy*. 2006; 13:541–552. [PubMed: 16397510]
37. Li X, Chen Y, Wang M, Ma Y, Xia W, Gu H. A mesoporous silica nanoparticle-PEI-fusogenic peptide system for siRNA delivery in cancer therapy. *Biomaterials*. 2013; 34:1391–1401. [PubMed: 23164421]
38. Meng H, Mai WX, Zhang H, Xue M, Xia T, Lin S, et al. Codelivery of an optimal drug/siRNA combination using mesoporous silica nanoparticles to overcome drug resistance in breast cancer in vitro and in vivo. *ACS Nano*. 2013; 7:994–1005. [PubMed: 23289892]
39. Lin D, Cheng Q, Jiang Q, Huang Y, Yang Z, Han S, et al. Intracellular cleavable poly(2-dimethylaminoethyl methacrylate) functionalized mesoporous silica nanoparticles for efficient siRNA delivery in vitro and in vivo. *Nanoscale*. 2013; 5:4291–4301. [PubMed: 23552843]
40. Shen J, Kim HC, Su H, Wang F, Wolfram J, Kirui D, et al. Cyclodextrin and polyethylenimine functionalized mesoporous silica nanoparticles for delivery of siRNA cancer therapeutics. *Theranostics*. 2014; 4:487–497. [PubMed: 24672582]
41. Ngamcherdtrakul W, Morry J, Gu S, Castro DJ, Goodyear SM, Sangvanich T, et al. Cationic Polymer Modified Mesoporous Silica Nanoparticles for Targeted siRNA Delivery to HER2+ Breast Cancer. *Advanced Functional Materials*. 2015; 25:2646–2659. [PubMed: 26097445]
42. Ishida, Y.; Nagata, K. Chapter nine - Hsp47 as a Collagen-Specific Molecular Chaperone. In: James, CW.; Phillip, IB., editors. *Methods in enzymology*. Academic Press; 2011. p. 167-182.
43. Kuroda K, Tsukifuji R, Shinkai H. Increased expression of heat-shock protein 47 is associated with overproduction of type I procollagen in systemic sclerosis skin fibroblasts. *The Journal of investigative dermatology*. 1998; 111:1023–1028. [PubMed: 9856811]
44. Naitoh M, Hosokawa N, Kubota H, Tanaka T, Shirane H, Sawada M, et al. Upregulation of HSP47 and collagen type III in the dermal fibrotic disease, keloid. *Biochemical and biophysical research communications*. 2001; 280:1316–1322. [PubMed: 11162672]
45. Razzaque MS, Kumatori A, Harada T, Taguchi T. Coexpression of collagens and collagen-binding heat shock protein 47 in human diabetic nephropathy and IgA nephropathy. *Nephron*. 1998; 80:434–443. [PubMed: 9832643]
46. Amenomori M, Mukae H, Sakamoto N, Kakugawa T, Hayashi T, Hara A, et al. HSP47 in lung fibroblasts is a predictor of survival in fibrotic nonspecific interstitial pneumonia. *Respiratory medicine*. 2010; 104:895–901. [PubMed: 20129768]
47. Brown KE, Broadhurst KA, Mathahs MM, Brunt EM, Schmidt WN. Expression of HSP47, a collagen-specific chaperone, in normal and diseased human liver. *Laboratory investigation; a journal of technical methods and pathology*. 2005; 85:789–797.
48. Sato Y, Murase K, Kato J, Kobune M, Sato T, Kawano Y, et al. Resolution of liver cirrhosis using vitamin A-coupled liposomes to deliver siRNA against a collagen-specific chaperone. *Nature biotechnology*. 2008; 26:431–442.
49. Ishiwatari H, Sato Y, Murase K, Yoneda A, Fujita R, Nishita H, et al. Treatment of pancreatic fibrosis with siRNA against a collagen-specific chaperone in vitamin A-coupled liposomes. *Gut*. 2013; 62:1328–1339. [PubMed: 23172890]
50. Obata Y, Nishino T, Kushibiki T, Tomoshige R, Xia Z, Miyazaki M, et al. HSP47 siRNA conjugated with cationized gelatin microspheres suppresses peritoneal fibrosis in mice. *Acta biomaterialia*. 2012; 8:2688–2696. [PubMed: 22487929]
51. Leachman SA, Hickerson RP, Schwartz ME, Bullough EE, Hutcherson SL, Boucher KM, et al. First-in-human Mutation-targeted siRNA Phase Ib Trial of an Inherited Skin Disorder. *Molecular*

therapy : the journal of the American Society of Gene Therapy. 2009; 18:442–446. [PubMed: 19935778]

52. Yamamoto T, Takagawa S, Katayama I, Yamazaki K, Hamazaki Y, Shinkai H, et al. Animal model of sclerotic skin. I: Local injections of bleomycin induce sclerotic skin mimicking scleroderma. *The Journal of investigative dermatology*. 1999; 112:456–462. [PubMed: 10201529]
53. Takashima A. Establishment of fibroblast cultures. *Curr Protoc Cell Biol*. 2008/01/30 ed2001. p. 2.1. - 2.1.12.
54. Boucherat O, Franco-Montoya ML, Thibault C, Incitti R, Chailley-Heu B, Delacourt C, et al. Gene expression profiling in lung fibroblasts reveals new players in alveolarization. *Physiol Genomics*. 2007; 32:128–141. [PubMed: 17911382]
55. Yamamoto T, Nishioka K. Animal model of sclerotic skin. V: Increased expression of alpha-smooth muscle actin in fibroblastic cells in bleomycin-induced scleroderma. *Clin Immunol*. 2002; 102:77–83. [PubMed: 11781070]
56. Brand-Williams W, Cuvelier ME, Berset C. Use of a free radical method to evaluate antioxidant activity. *LWT - Food Science and Technology*. 1995; 28:25–30.
57. Jacobson GB, Gonzalez-Gonzalez E, Spitler R, Shinde R, Leake D, Kaspar RL, et al. Biodegradable nanoparticles with sustained release of functional siRNA in skin. *Journal of Pharmaceutical Sciences*. 2010; 99:4261–4266. [PubMed: 20737633]
58. Hegde V, Hickerson RP, Nainamalai S, Campbell PA, Smith FJD, McLean WHI, et al. In vivo gene silencing following non-invasive siRNA delivery into the skin using a novel topical formulation. *Journal of Controlled Release*. 2014; 196:355–362. [PubMed: 25449884]
59. Loor G, Kondapalli J, Schriewer JM, Chandel NS, Vanden Hoek TL, Schumacker PT. Menadiione triggers cell death through ROS-dependent mechanisms involving PARP activation without requiring apoptosis. *Free radical biology & medicine*. 2010; 49:1925–1936. [PubMed: 20937380]
60. Read ML, Singh S, Ahmed Z, Stevenson M, Briggs SS, Oupicky D, et al. A versatile reducible polycation-based system for efficient delivery of a broad range of nucleic acids. *Nucleic acids research*. 2005; 33:e86. (1–16). [PubMed: 15914665]
61. Kawakami T, Ihn H, Xu W, Smith E, LeRoy C, Trojanowska M. Increased expression of TGF-beta receptors by scleroderma fibroblasts: evidence for contribution of autocrine TGF-beta signaling to scleroderma phenotype. *The Journal of investigative dermatology*. 1998; 110:47–51. [PubMed: 9424086]
62. Sambo P, Baroni SS, Luchetti M, Paroncini P, Dusi S, Orlandini G, et al. Oxidative stress in scleroderma: maintenance of scleroderma fibroblast phenotype by the constitutive up-regulation of reactive oxygen species generation through the NADPH oxidase complex pathway. *Arthritis and rheumatism*. 2001; 44:2653–2664. [PubMed: 11710721]
63. Pohlers D, Brenmoehl J, Loffler I, Muller CK, Leipner C, Schultze-Mosgau S, et al. TGF-beta and fibrosis in different organs - molecular pathway imprints. *Biochimica et biophysica acta*. 2009; 1792:746–756. [PubMed: 19539753]
64. Xu Q, Norman JT, Shrivastav S, Lucio-Cazana J, Kopp JB. In vitro models of TGF-beta-induced fibrosis suitable for high-throughput screening of antifibrotic agents. *American journal of physiology Renal physiology*. 2007; 293:F631–F640. [PubMed: 17494090]
65. Lakos G, Takagawa S, Chen S-J, Ferreira AM, Han G, Masuda K, et al. Targeted Disruption of TGF-β/Smad3 Signaling Modulates Skin Fibrosis in a Mouse Model of Scleroderma. *The American journal of pathology*. 2004; 165:203–217. [PubMed: 15215176]
66. Oi M, Yamamoto T, Nishioka K. Increased expression of TGF-beta1 in the sclerotic skin in bleomycin-'susceptible' mouse strains. *J Med Dent Sci*. 2004; 51:7–17. [PubMed: 15137460]
67. Hong S-Y, Gil H-W, Yang J-O, Lee E-Y, Kim H-K, Kim S-H, et al. Effect of High-Dose Intravenous N-acetylcysteine on the Concentration of Plasma Sulfur-Containing Amino Acids. *The Korean Journal of Internal Medicine*. 2005; 20:217–223. [PubMed: 16295780]
68. Sasaki H, Sato T, Yamauchi N, Okamoto T, Kobayashi D, Iyama S, et al. Induction of heat shock protein 47 synthesis by TGF-β and IL-1β via enhancement of the heat shock element binding activity of heat shock transcription factor 1. *The Journal of Immunology*. 2002; 168:5178–5183. [PubMed: 11994473]

69. Chan EC, Peshavariya HM, Liu G-S, Jiang F, Lim S-Y, Dusting GJ. Nox4 modulates collagen production stimulated by transforming growth factor β 1 in vivo and in vitro. *Biochemical and biophysical research communications*. 2013; 430:918–925. [PubMed: 23261430]
70. Jiang F, Liu G-S, Dusting GJ, Chan EC. NADPH oxidase-dependent redox signaling in TGF- β -mediated fibrotic responses. *Redox Biology*. 2014; 2:267–272. [PubMed: 24494202]
71. Barnes JL, Gorin Y. Myofibroblast differentiation during fibrosis: role of NAD(P)H oxidases. *Kidney international*. 2011; 79:944–956. [PubMed: 21307839]
72. Yu AL, Moriniere J, Birke M, Neumann C, Fuchshofer R, Kampik A, et al. Reactivation of Optic Nerve Head Astrocytes by TGF- β 2 and H₂O₂ Is Accompanied by Increased Hsp32 and Hsp47 Expression. *Investigative Ophthalmology & Visual Science*. 2009; 50:1707–1717. [PubMed: 18952926]
73. Gosslau A, Ruoff P, Mohsenzadeh S, Hobohm U, Rensing L. Heat shock and oxidative stress-induced exposure of hydrophobic protein domains as common signal in the induction of hsp68. *J Biol Chem*. 2001; 276:1814–1821. [PubMed: 11042186]
74. Sikić BI. Biochemical and cellular determinants of bleomycin cytotoxicity. *Cancer surveys*. 1986; 5:81–91. [PubMed: 2439200]

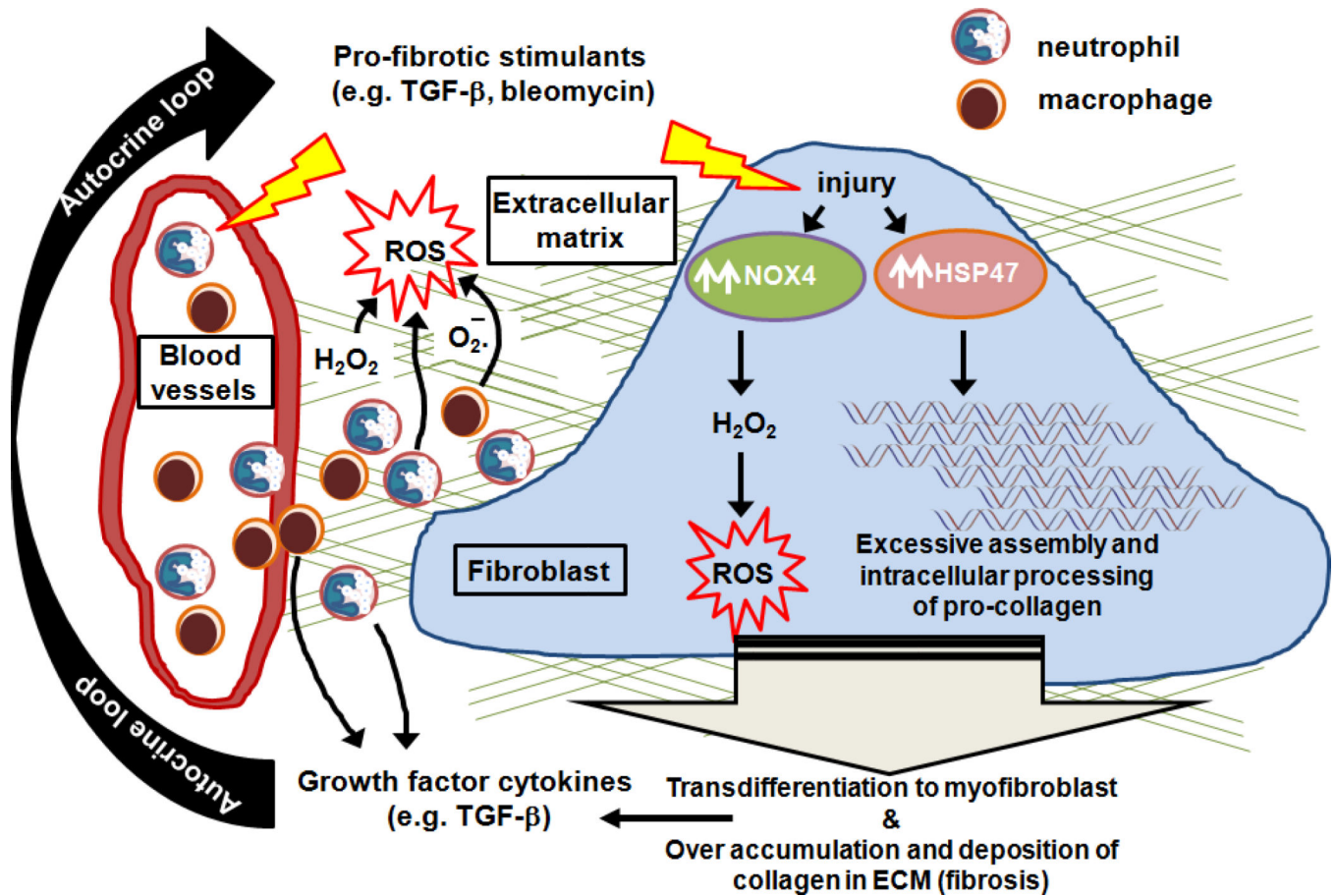


Figure 1. Schematic illustrating pathogenesis of fibrosis. Pro-fibrotic stimulants (e.g., TGF- β or bleomycin) activate macrophages and neutrophils to secrete pro-fibrotic cytokines (e.g., TGF- β) and ROS (e.g., H_2O_2 , superoxide) into the extracellular matrices (ECM) and surrounding cells. The presence of cytokines and ROS leads to up-regulation of profibrotic genes (NOX4, HSP47, α -SMA, and COL I) in fibroblast cells, transdifferentiation of quiescent fibroblast cells to myfibroblasts, and over-accumulation of collagen in the ECM, leading to fibrosis. Myfibroblasts will secrete more TGF- β , further inducing fibrogenesis in an autocrine loop.

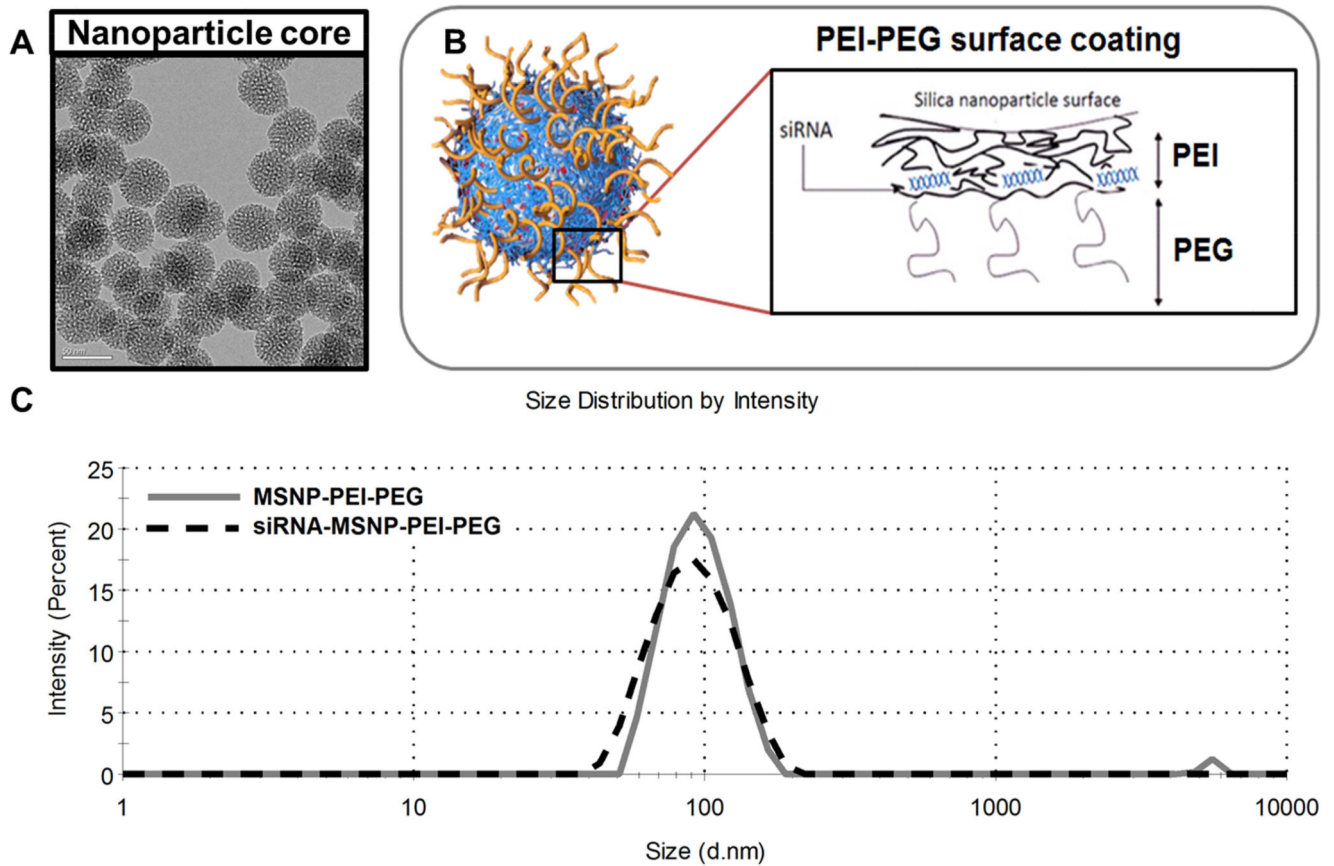


Figure 2. MSNP-PEI-PEG nanoparticle. (A) TEM image of the mesoporous silica nanoparticle (MSNP) core (scale bar = 50 nm). (B) Schematic of surface modification of MSNP (layer-by-layer) with polyethyleneimine (PEI), polyethyleneglycol (PEG), and siRNA. (C) Hydrodynamic size distribution of MSNP-PEI-PEG (solid line) and with siRNA loading (dashed line).

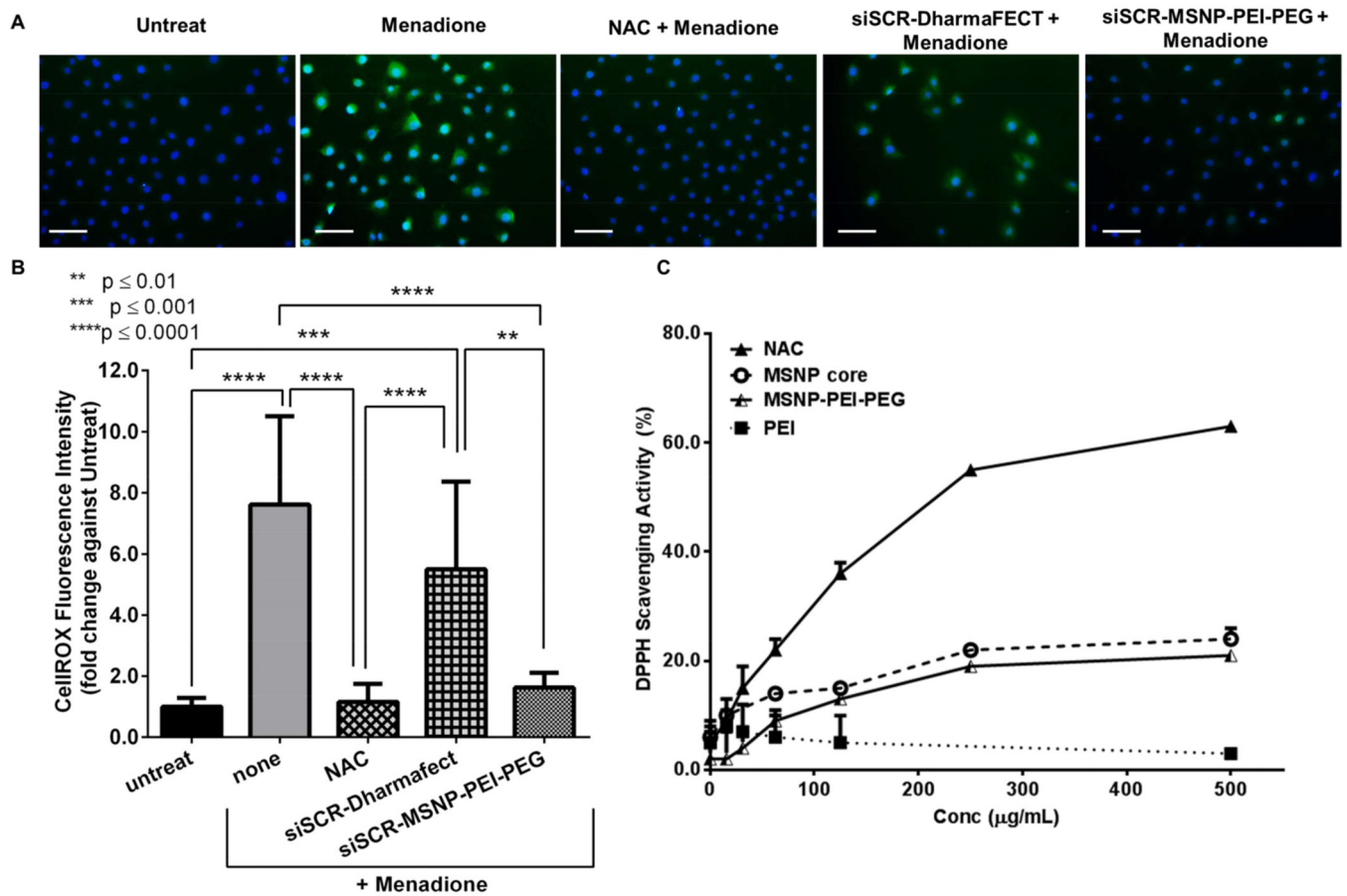


Figure 3. Intracellular ROS activity of primary dermal fibroblast treated for 24 hr with NAC (2 mM), siSCR-MSN-PEI-PEG (17.5 µg/mL nanoparticles, 50 nM siSCR) or siSCR-DharmaFECT (0.5 µL/well, 50 nM siSCR, 100 µL volume), followed by 1-hr treatment with 100 µM menadione. (A) Representative images of cells (Hoechst dye, blue) stained with CellROX (green), scale bar = 100 µm. (B) Corresponding CellROX fluorescence intensity normalized by cell number (Hoechst-positive) and reported as fold changes against untreated control. (C) DPPH scavenging activity of various materials in a cell-free system.

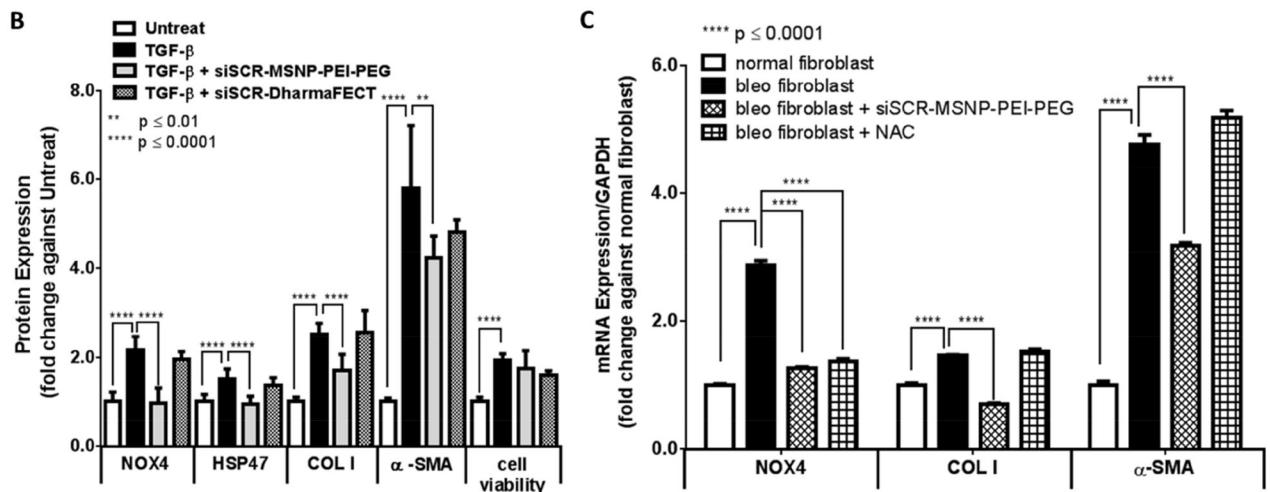
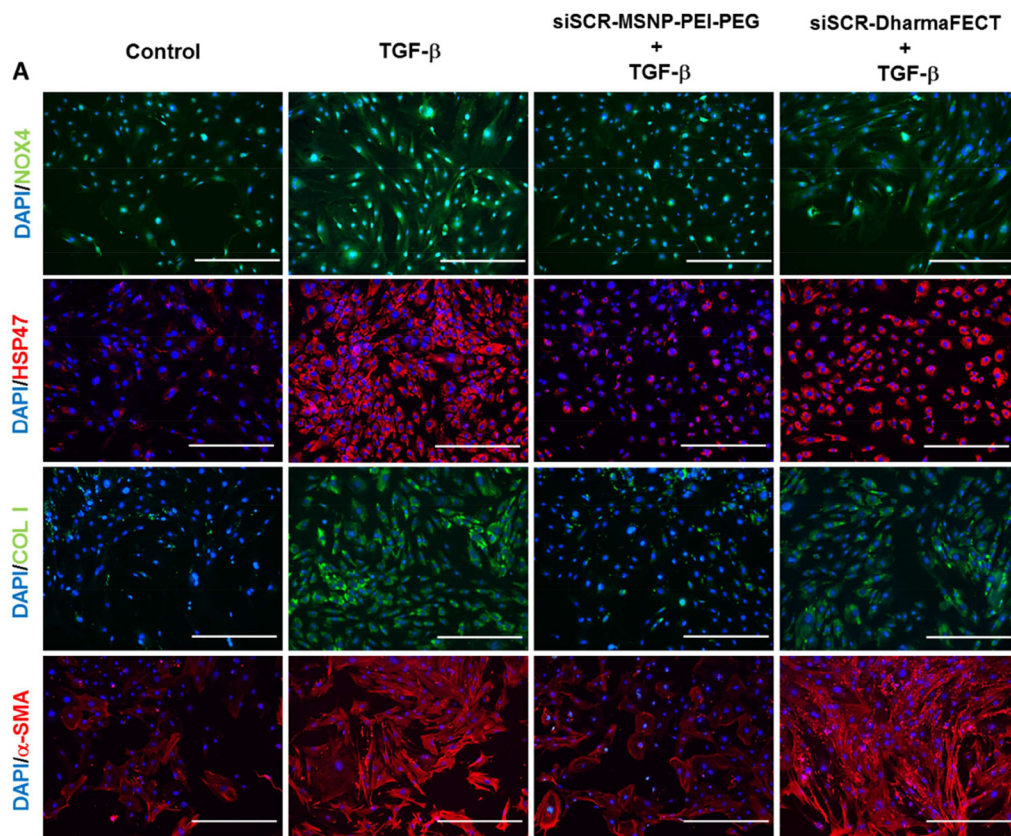


Figure 4.

NOX4-modulating effects of MSNP-PEI-PEG on TGF- β -stimulated and scleroderma-like dermal fibroblast cells. (A) Representative images of the TGF- β -stimulated cells stained for NOX4, HSP47, COL I, and α -SMA after 24-hr treatment with siSCR-MSNP-PEI-PEG or siSCR-DharmaFECT, followed by 72-hr treatment with 10 ng/mL TGF- β , scale bar = 400 μ m. (B) Corresponding protein intensity normalized by cell number (DAPI), reported as fold changes against the untreated control, and cell viability after each treatment. (C) mRNA expressions following 48-hr treatment with MSNP-PEI-PEG nanoparticles (17.5 μ g/mL, 50

nM siSCR) vs. NAC (2 mM) on murine dermal fibroblasts harvested from bleomycin-induced scleroderma mouse model (bleo-fibroblast).

Author Manuscript

Author Manuscript

Author Manuscript

Author Manuscript

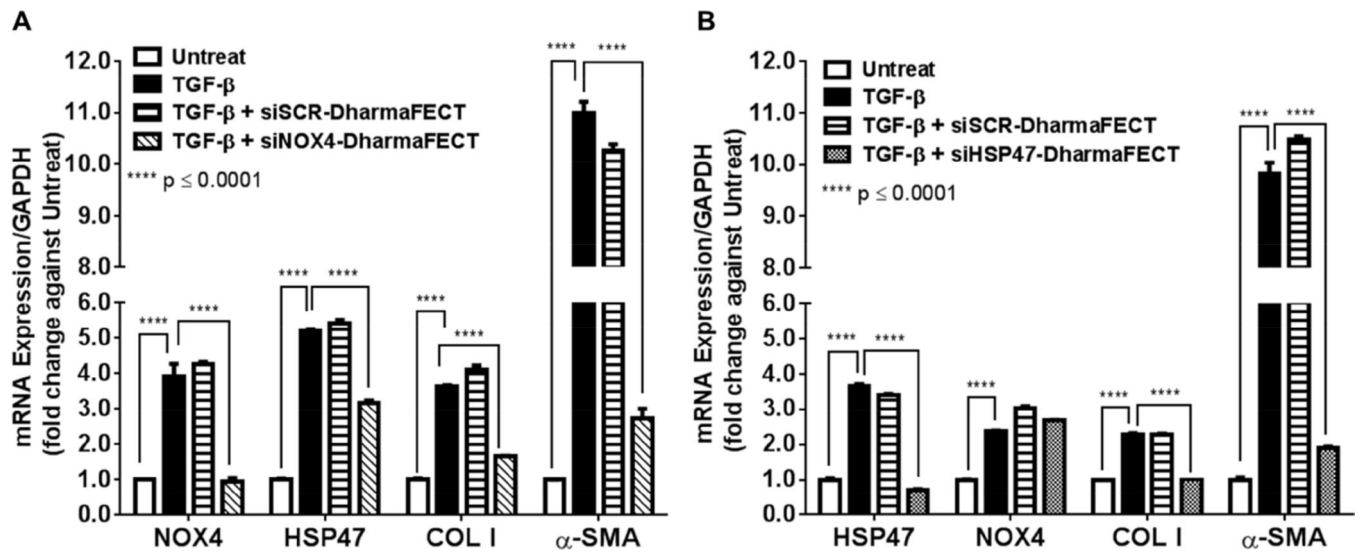


Figure 5.

In vitro siNOX4 or siHSP47 transfection with DharmaFECT. mRNA expression of primary dermal fibroblast cells treated for 24 hr with (A) siRNA against NOX4 (siNOX4) or (B) siRNA against HSP47 (siHSP47) vs. non-targeting siRNA (siSCR), followed by 24 hr of 10 ng/mL TGF- β stimulation. siRNA dose of 50 nM in 0.5 μ L/well DharmaFECT.

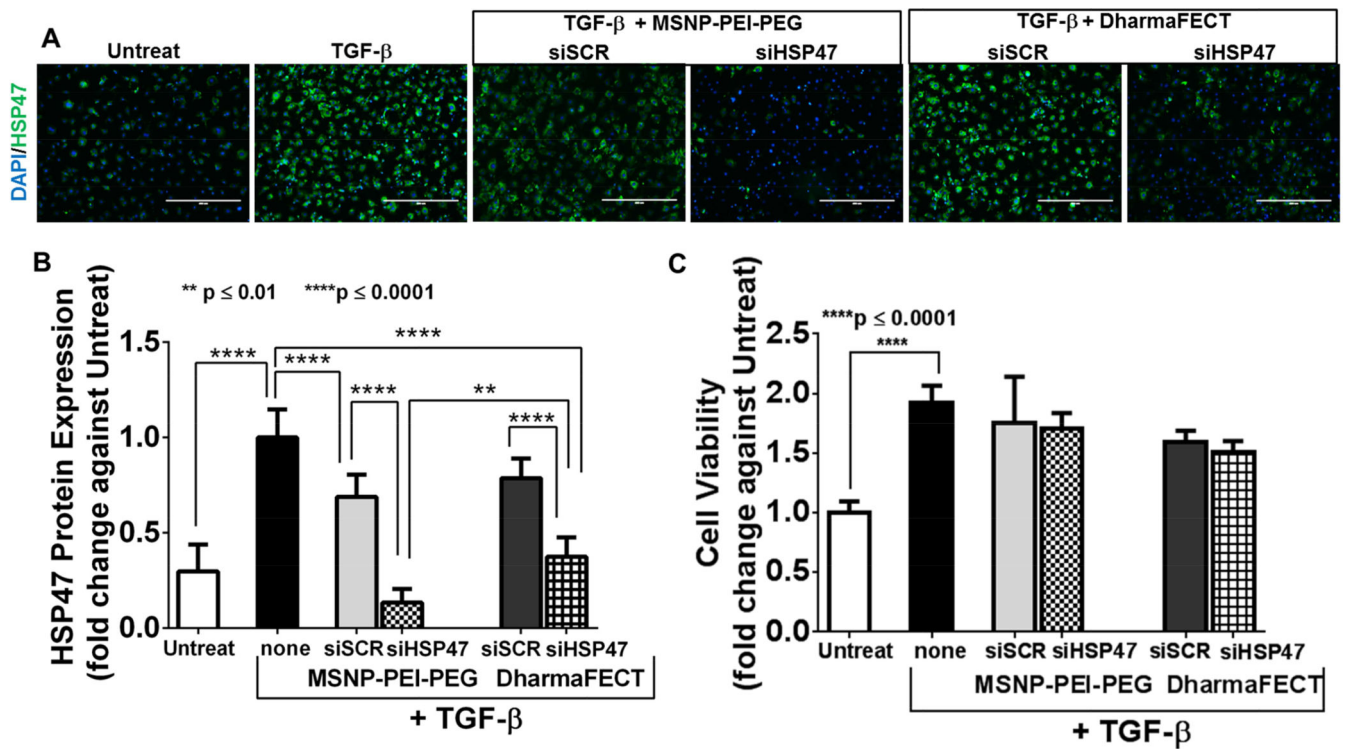


Figure 6.

In vitro gene silencing efficacy with siHSP47-MSNP-PEI-PEG nanoparticles. (A) Representative images of HSP47 stain on primary murine dermal fibroblast treated for 24 hr with siHSP47-MSNP-PEI-PEG or siHSP47-DharmaFECT, followed by 72 hr of 10 ng/mL TGF- β stimulation. Scale bar = 400 nm. (B) Corresponding HSP47 protein expression normalized by cell number (DAPI) and reported as fold change against the untreated control. (C) Relative cell viability upon the same treatments with (B).

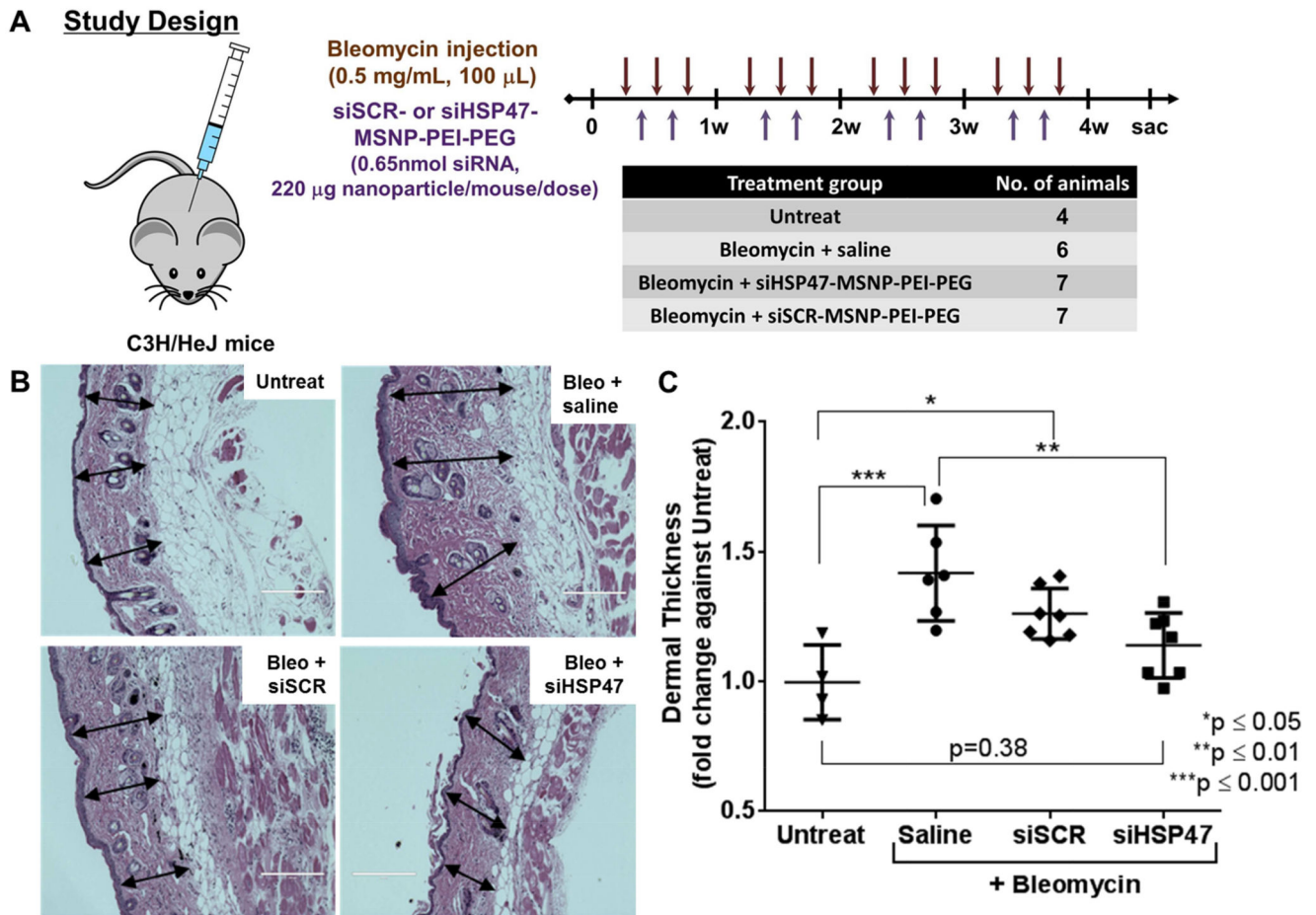


Figure 7. Effect of siHSP47-MSNP-PEI-PEG nanoparticles on dermal thickness in the bleomycin-induced scleroderma mouse model. (A) Dosing scheme of bleomycin induction and the siHSP47-MSNP-PEI-PEG treatment. (B) Representative images of skin sections stained with hematoxylin and eosin (H&E), scale bar = 200 μ m. (C) Dermal thickness measured from skin sections as in (C).

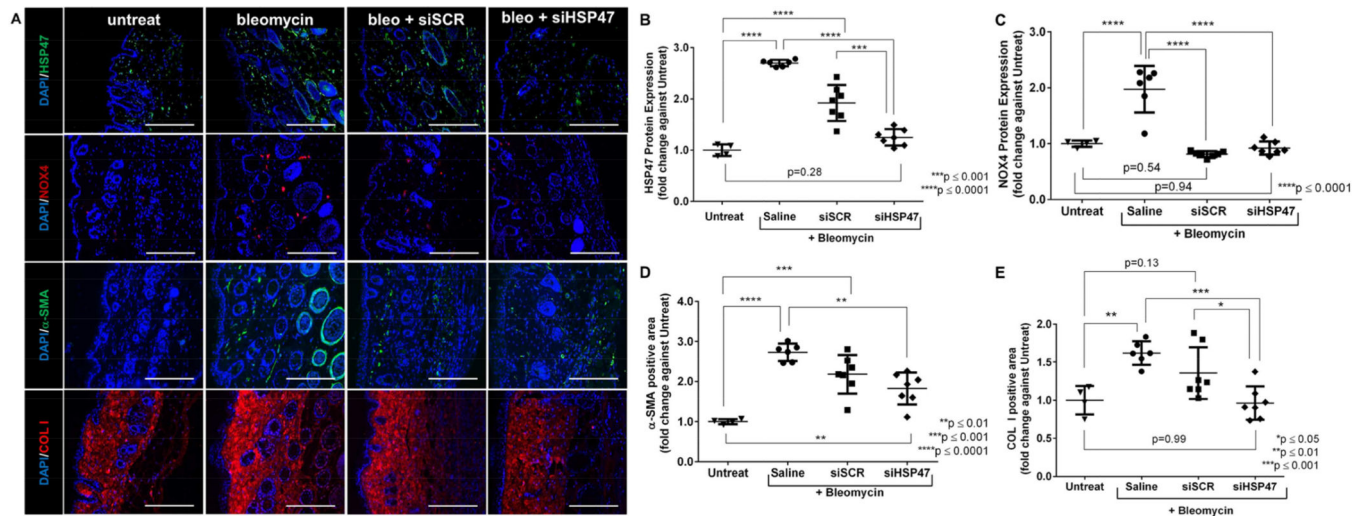


Figure 8. HSP47 silencing efficacy and anti-fibrotic effects of siHSP47-MSN-PEI-PEG nanoparticles on bleomycin-induced scleroderma mouse model (dosing scheme as specified in Fig. 7A). (A) Representative images of skin sections stained with HSP47, NOX4, α -SMA, and COL I. Nuclei were stained with DAPI, scale bar = 200 μ m. Expression levels of (B) HSP47 and (C) NOX4 proteins as well as (D) α -SMA- and (E) COL I-positive area were quantified by immunofluorescence analysis, normalized by that of untreated control.